

Influence of substrate surface-grinding on surface roughness of zirconia coatings fabricated by room temperature spray processing

Jeong Jun Kim and Jong Kook Lee*

Department of Advanced Materials and Engineering, Chosun University, Gwangju 61452, Korea

Zirconia ceramics used for dental implants have low bioactivity. Their surface roughness needs to be enhanced for improved bone-bonding ability and cell adhesion. Zirconia implants in the gums with low surface roughness have a probability detachment over time. In this study, a zirconia substrate zirconia was coated by a powder via spray processing at room temperature (25 °C) to increase its surface roughness. In addition, we investigated the morphology of the as-produced rough substrate, including microstructural evolution. Four types of zirconia substrates with different surface texture were fabricated via surface-grinding by silicon carbide (SiC) abrasive papers (#220, #400, #800) after sintering. Room temperature spray processing was carried out using a commercial zirconia powder after thermal treatment. The as-produced zirconia coatings showed dense microstructure and uniform thickness. Surface roughness of zirconia substrate was greatly enhanced depending on the surface texture of the substrate. Surface texture by substrate grinding affected coating morphology; however, it did not increase the surface roughness of the substrate or the coatings. High-roughened coatings and thick coating layer could be obtained from the as-sintered substrate owing to its high surface roughness.

Keywords: Zirconia substrate, Room temperature spray processing, Surface roughness.

Introduction

3 mol% yttria-stabilized tetragonal zirconia polycrystals (3Y-TZP) exhibits superior mechanical properties such as high fracture toughness ($\sim 10 \text{ MPa}\cdot\text{m}^{-1/2}$), high flexural strength ($\sim 1,300 \text{ MPa}$), elastic modulus ($\sim 210 \text{ GPa}$), and abrasion resistance ($\sim 1,200 \text{ Hv}$) [1-4]. It also characterized by biological and optical properties, for example, good biocompatible properties, i.e., corrosion resistance, non-toxicity, minimal ion release, low affinity to bacterial colonization, and good esthetics [5, 6]. The mechanical, biological and optical properties of zirconia dental implants are related to the ionic and phase composition, hydrophilicity, and surface roughness, which depend on the bulk composition as well as the surface treatment of the implants [7, 8]. Even though 3 mol% yttria-stabilized tetragonal zirconia (3Y-TZP) is the most commonly used material, yttria content of zirconia bulk materials can vary from 3 to 5 mol% [9, 10].

Most of zirconia implants are fabricated by the milling of ceramic block using a computer-aided design and computer-aided manufacturing (CAD/CAM) system, after post-sintering [11]. Shaping of zirconia blocks by cutting or grinding creates several invisible microcracks on the machined implant surface that might induce microstructural disintegration or failure after implantation,

limiting the use of this material as a dental implant [12, 13]. Fabrication of zirconia implants by CAD/CAM and sintering usually results in a relatively smooth surface, that reduces its bone-bonding ability and cell adhesion [14, 15].

The surface treatment of zirconia dental implants is diverse and has not been thoroughly studied. Several efforts have been made to roughen the zirconia implant surface to improve its osseointegration. Numerous surface modifications are currently being applied, such as sandblasting and acid etching to enhance the surface roughness of CAD/CAM machined zirconia implants [16, 17]. Zirconia particles are also used as an effective coating material, and surface coating is a frequently used method to improve the surface roughness and bone-bonding ability of dental zirconia implants [18, 19].

In this study, we applied a zirconia coating on zirconia substrate to obtain a highly roughened zirconia surface by spray processing at room temperature (25 °C), to improve the bone-bonding ability and osseointegration of the implant. We also investigated the effect of substrate texturing and roughness on coating morphology, including microstructural evolution, surface roughness, and coating thickness.

Experimental Details

Materials

Commercial 3Y-TZP powder was used as the raw material to fabricate the zirconia coating and substrate. To match the processing condition for room temperature

*Corresponding author:
Tel : +82-62-230-7202
Fax: +82-62-608-5402
E-mail: jklee@chosun.ac.kr

spray processing, 3Y-TZP powder was heat-treated at 1,100 °C for 2 h to enlarge the particle size and weight. After calcination, attrition-milling was performed for 24 h. After drying, the powder was sieved to prevent the nozzle from clogging during coating.

Dense zirconia substrate 1 cm in diameter was fabricated by uniaxial pressing and sintering at 1,450 °C for 2 h. Surface microstructure and roughness of substrate were investigated via field emission scanning electron microscopy (FE-SEM) and atomic force microscopy (AFM). To change the surface texture of the zirconia substrate, abrasive milling was performed using the three types of silicon carbide (SiC) paper (#220, #400, #800).

Coating

The 3Y-TZP substrate was coated with zirconia particles by spray processing at room temperature. A few preliminary experiments were performed to determine the optimum coating parameters as described in our previous study [20]. Pressure difference between aerosol and deposition chambers was maintained at 1 atm under the nitrogen gas flow rate of 5 L/min. The distance between the nozzle and the substrate, termed as spraying distance, was set at 5 mm. Aerosol of 3Y-TZP particles in the deposition chamber was formed by the injection of nitrogen gas and severe vibrations at approximately 600 rpm. The 3Y-TZP particles carried via nitrogen flow into the deposition chamber were rapidly impacted onto the substrate and deposited as the coating layer. To obtain a thick coating on the substrate, coating cycle was repeated a maximum of 40 times in succession, using a slit nozzle with a size of 15 × 1 mm². Detailed experimental procedure for the preparation of substrate and room temperature spray processing is indicated in Fig. 1.

Characterization

The change in the color of the coating with deposition cycle was observed using optical microscope, and its phase composition was analyzed by X-ray diffraction (XRD). The morphology and microstructure of the coated layer were investigated both on planar and perpendicular surfaces using an FE-SEM. Coating thickness was measured as a function of the deposition cycle and the values were compared based on the degree of surface-grinding. Surface morphology and microstructure of the 3Y-TZP coating were observed by SEM and AFM and investigated with respect to the deposition cycle and surface-grinding type. From the AFM image, the roughness parameter (Ra; centerline average roughness) was measured, and the relation between coating properties and processing parameters was analyzed.

Results and Discussion

Heat treatment of the 3Y-TZP powder at high temperature is essential to obtain the powder that is suitable for spray coating at room temperature; it also provides sufficient impaction energy to the particles for collision [21, 22]. All 3Y-TZP particles after calcination showed an equiaxed shape with uniform agglomeration as shown in Fig. 2(a). From the analysis of particle size distribution (Fig. 2(b)), calcined 3Y-TZP powder had primary and secondary agglomerate sizes of 287 nm and 3.3 μm, respectively, and composed of 75 vol% primary and 25 vol% secondary agglomerates. Calcined and milled 3Y-TZP powder was characterized as the main tetragonal phase with a trace of monoclinic phase as per the XRD analysis (Fig. 2(c)), indicating partial phase transformation by heat-treatment and attrition milling.

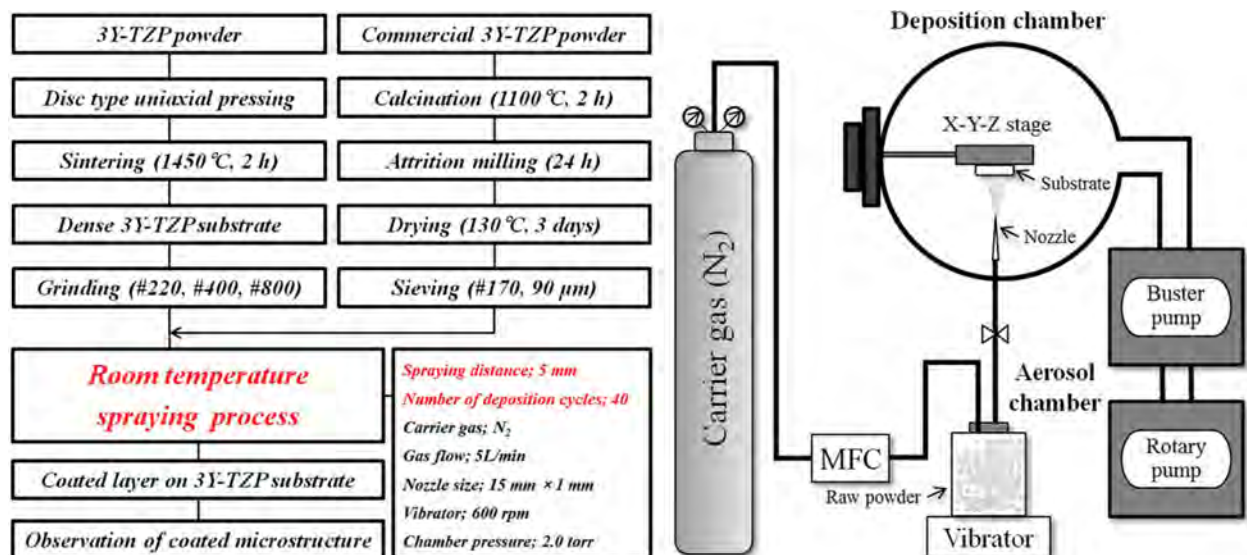


Fig. 1. Schematic for the preparation of 3Y-TZP coating powder and substrate, and the room temperature spray processing.

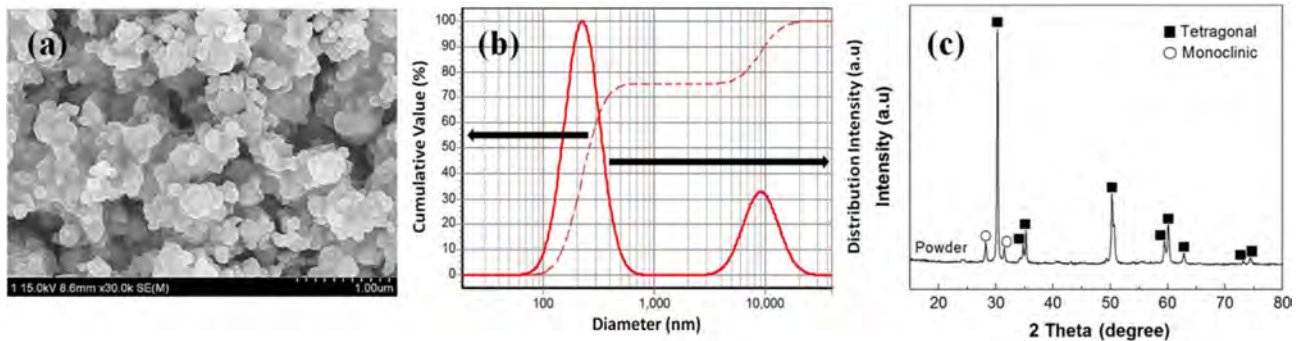


Fig. 2. Characterization of coating powder after calcination; (a) particle morphology, (b) agglomeration size distribution and (c) phase composition.

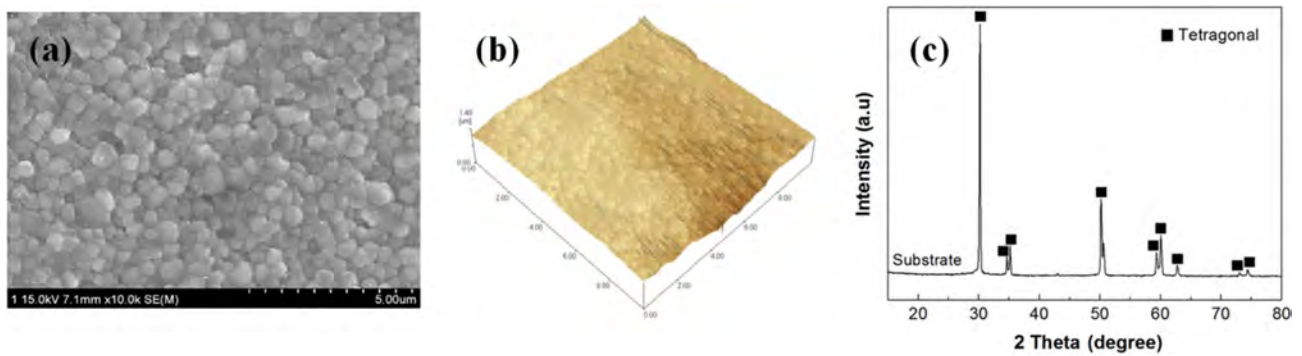


Fig. 3. Characterization of the as-sintered 3Y-TZP substrate before surface-grinding; (a) surface microstructure as per SEM, (b) surface morphology as per AFM, and (c) phase composition.

Surface microstructure and morphology of the as-sintered 3Y-TZP substrate observed by SEM and AFM are shown in Fig. 3, indicating that the specimen has homogeneous microstructure composed of all tetragonal grains of 500 nm, and 0.28 μm surface roughness (R_a) measured from AFM image. Fig. 4 shows the surface morphology and roughness of the 3Y-TZP substrate after surface-grinding by three types of SiC abrasive. Several scratches in vertical direction were observed from the SEM photographs, but the scale and frequency of scratches were dependent on the type of the SiC abrasive. Surface-grinding by coarse SiC abrasive (#220) induced large scale scratches on the substrate surface with relatively low frequency. In contrast, surface-grinding by fine SiC abrasive (#800) greatly reduced the scratch mode on the substrate surface, resulting in low surface roughness (R_a). Even though large scratches were formed on the substrate surface by surface-grinding it caused a decrease in the roughness value (R_a) from 0.28 μm (as-sintered substrate) to 0.18 μm (#800 SiC abrasive).

Surface color of the as-sintered 3Y-TZP substrate corresponds to that of the ivory, which is the typical color of 3Y-TZP. After the coating of zirconia substrate by 3Y-TZP particles the color of the former changed to gray-black as shown in Fig. 5(a), depending on the deposition cycle and the type of surface-grinding. In a

previous study [23] dark gray or black color was generally observed in thick coating layer, and the color change was influenced by the carrier gas and the degree of coating thickness. The presence of gray-color on the coating layer was caused by the discharging during the deposition, which induced defects in the film and drastically decreased its transmittance [24]. Coated zirconia layer was composed of all tetragonal grains as indicated in Fig. 5(b), regardless of the type of surface-grinding. Trace of monoclinic phase in starting zirconia powder was not observed on coated zirconia layer, meaning that tetragonal grains were formed by strong impaction and adhesiveness on substrate during the room temperature spray processing.

Fig. 6 shows the surface microstructure and morphology of the coating layers fabricated by room temperature spray processing as a function of surface-grinding. No delamination or micro-cracks were observed in the coating layer or at the interface between the coating and substrate. All coating layers were composed of nanoscale 3Y-TZP particles in the range of 50 to 200 nm. Homogeneous surface microstructure and coating thickness was obtained for all substrates, but coating morphology and thickness were dependent on the texture of the substrate surface after grinding. Coated microstructure showed a three dimensional network or a wave-like pattern in the as-sintered specimens as well

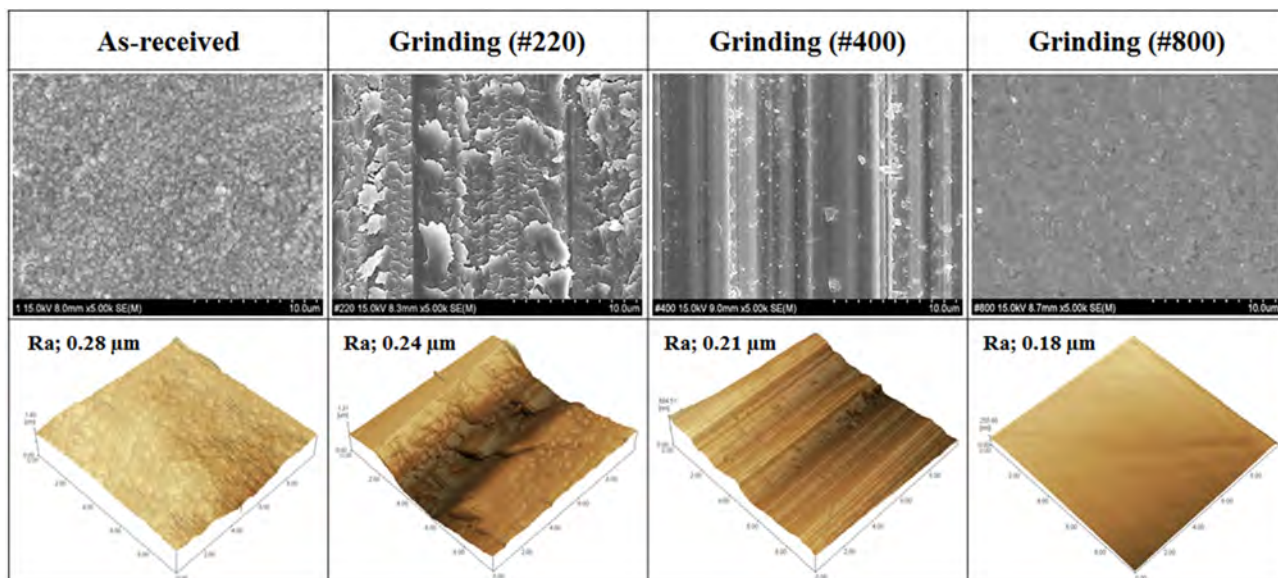


Fig. 4. Planar microstructure by SEM and surface morphology by AFM of 3Y-TZP substrates after surface-grinding.

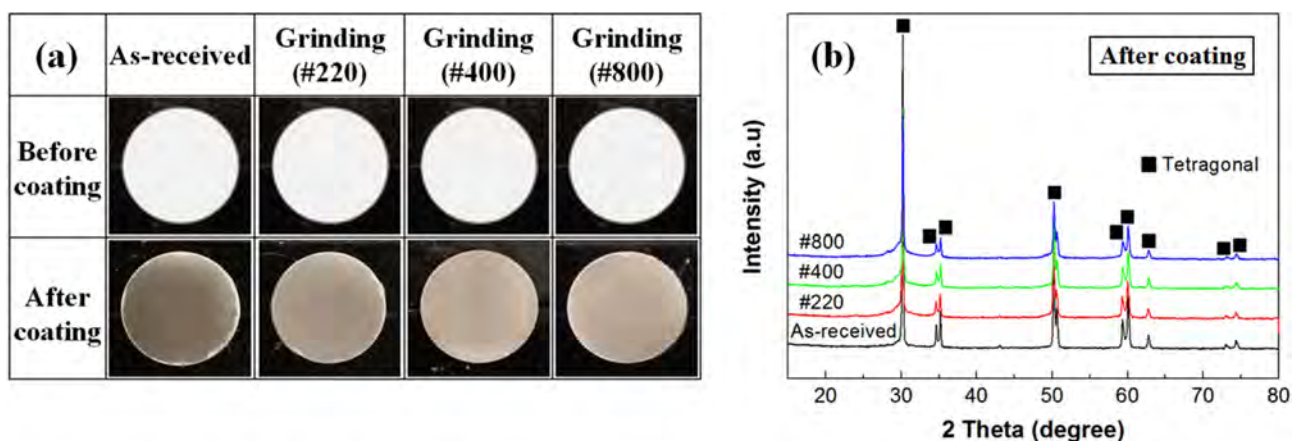


Fig. 5. Optical photographs and phase analysis of 3Y-TZP coatings as a function of deposition cycle and the type of surface-grinding: (a) color of coated layer and (b) phase composition.

as those obtained by fine grinding by #800 SiC abrasive; however, large difference in surface roughness were noted between the two coating layers. From the analysis of AFM images, maximum value of Ra ($0.42 \mu\text{m}$) was obtained for the coating layer of the as-sintered substrate; in contrast, minimum value of Ra ($0.32 \mu\text{m}$) was obtained from the coating layer of the specimen obtained by fine surface-grinding using #800 SiC abrasive.

Vertical lines were observed in the coated layers of the substrates with large scale scratches fabricated using #220, #400 SiC abrasive. In these specimens, coated morphology was similar to the vertical patterns on the substrate surface. The Ra of the coated layers gradually decreased from $0.42 \mu\text{m}$ to $0.32 \mu\text{m}$ with a decrease in the surface roughness of the substrate, indicating that highly roughened substrate is the main factor for

obtaining a highly roughened coating layer.

Fig. 7 shows the coating thickness and the surface roughness of the coated layer. The Ra of the coating layer can be calculated from the average value of the linear roughness data along the horizontal and vertical lines in the AFM map [25]. Coating thickness and surface roughness of the coated layer were also dependent on the substrate roughness based on the type of surface-grinding. Maximum coating thickness of $9.6 \mu\text{m}$ was observed for the coating layer of the as-sintered substrate. Conversely, minimum coating thickness of $3.2 \mu\text{m}$ was obtained for the coating layer of the substrate ground using #800 SiC abrasive.

Conclusions

Zirconia substrate was coated by zirconia particles by

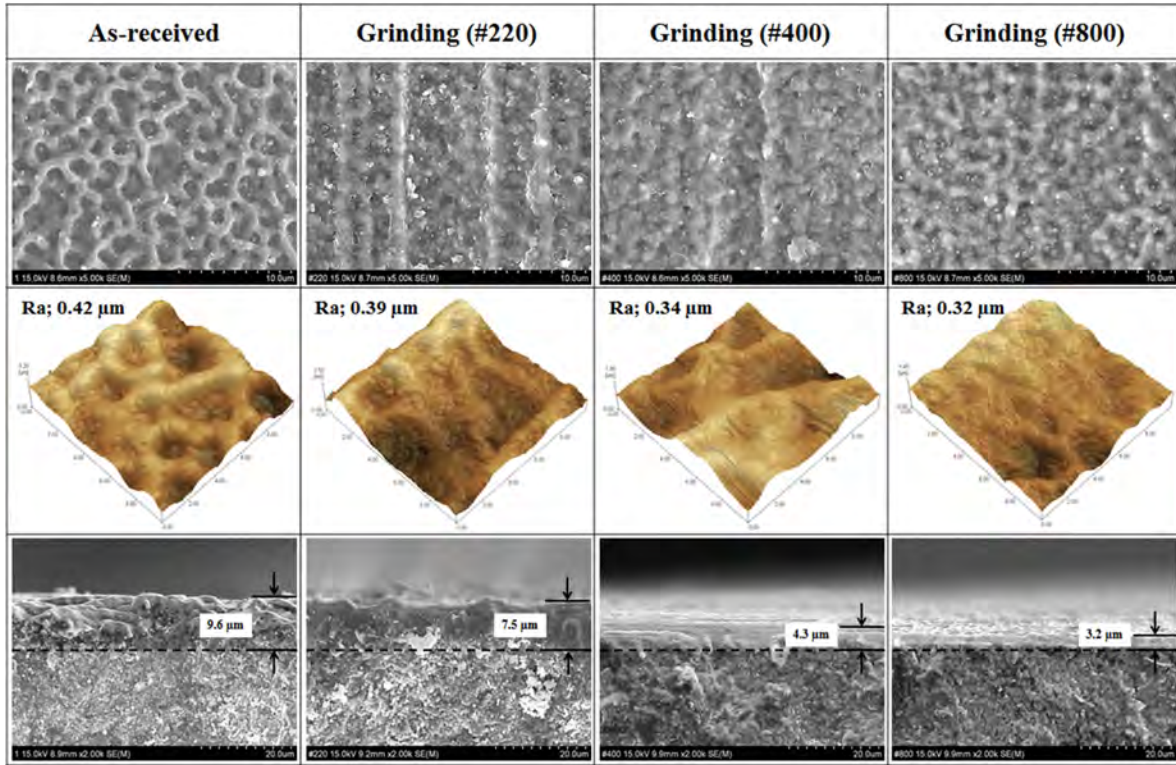


Fig. 6. Characterization of coated 3Y-TZP morphology by room temperature spray processing observed by SEM and AFM with respect to the type of substrate surface-grinding.

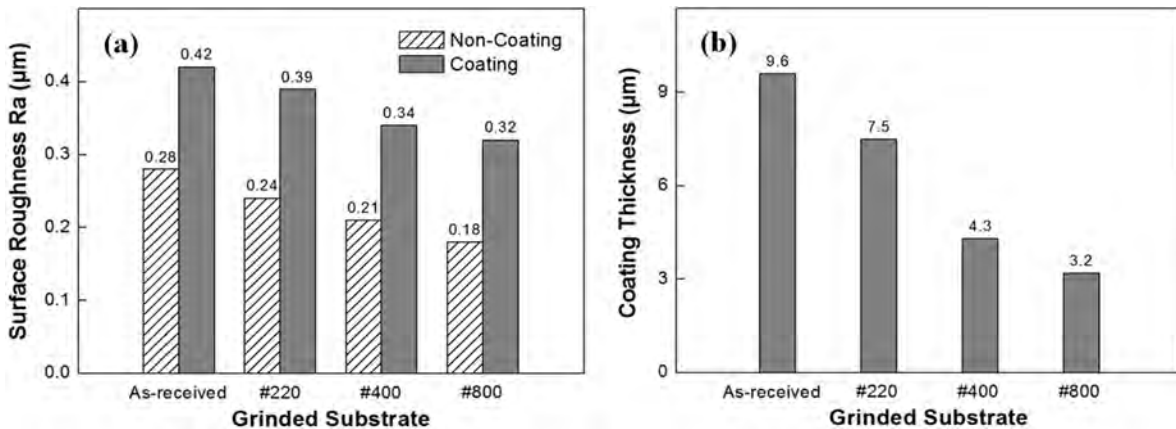


Fig. 7. Variations in (a) surface roughness determined via AFM images and (b) coating thickness determined from perpendicular images of SEM.

spraying process at room temperature to improve the bone-bonding ability and cell adhesion of zirconia dental implants by enhancing the surface roughness of the as-obtained specimens. The influence of substrate surface-grinding on the surface roughness of the coating surface was also investigated. Large and small scratches were induced on the zirconia substrate through surface-grinding by SiC abrasive, but the process resulted in decreased substrate roughness. Dense and homogeneous coatings composed of tetragonal zirconia grains were formed on the zirconia substrate by room temperature spray processing and coating morphology

and thickness were dependent on the substrate roughness and surface texture obtained by abrasive grinding. Maximum Ra of 0.42 μm and film thickness of 9.6 μm of the coated layer was obtained for the as-sintered substrate with maximum substrate roughness, indicating that a highly roughened coating layer adhered to the highly roughened substrate. In contrast, minimum surface roughness (Ra; 0.32 μm) and film thickness (3.2 μm) of the coated layer were obtained from the fine grinded substrate with minimum substrate roughness.

Acknowledgments

This work was supported by a National Research Foundation of Korea (NRF) grant funded by the Korea government (MEST) (Grant No. 2018-019041).

References

1. H. Nishihara, M.H. Adanez, and W. Att, *J. Prosthodont. Res.* 63[1] (2019) 1-14.
2. H. Tong, C.B. Tanaka, M.R. Kaizer, and Y. Zhang, *Ceram. Int.* 42[1] (2016) 1077-1085.
3. C. Gautam, J. Joyner, A. Gautam, J. Rao, and R. Vajtai, *Dalton. Trans.* 45[48] (2016) 19194-19215.
4. A. Apratim, P. Eachempati, K.K.K. Salian, V. Singh, S. Chhabra, and S. Shah, *J. Int. Soc. Prev. Community. Dent.* 5[3] (2015) 147-156.
5. E.S. Elshazly, S.M. El-Hout, and M.E.S. Ali, *J. Mater. Sci. Technol.* 27[4] (2011) 332-337.
6. I. Denry, and J.A. Holloway, *Mater.* 3[1] (2010) 351-368.
7. Y.R. Fonseca, C.N. Elias, S.N. Monteiro, H.E.S dos Santos, and C. Santos, *Mater.* 12[16] (2019) 2529.
8. F. Rupp, L. Liang, J. Geis-Gerstorfer, L.Scheideler, and F. Hüttig, *Dent. Mater.* 34[1] (2018) 40-57.
9. Z. Özkurt, and E. Kazazoğlu, *J. Oral. Implantol.* 37[3] (2011) 367-376.
10. M. Andreiotelli, H.J. Wenz, and R.J. Kohal, *Clin. Oral. Impl. Res.* 20[4] (2009) 32-47.
11. P.F. Manicone, P.R. Iommetti, and L. Raffaelli, *J. Dent.* 35[11] (2007) 819-826.
12. R. Depprich, C. Naujoks, M. Ommerborn, F. Schwarz, N.R. Kübler, and J. Handschel, *Clin. Implant. Dent. Relat. Res.* 16[1] (2014) 124-137.
13. Y. Zhang, and B.R. Lawn, *J. Biomed. Mater. Res. Part B Appl. Biomater.* 72B[2] (2005) 388-392.
14. G. Soon, B. Pingguan-Murphy, K.W. Lai, and S.A. Akbar, *Ceram. Int.* 42[11] (2016) 12543-12555.
15. M.R. Towler, I.R. Gibson, and S.M. Best, *J. Mater. Sci. Lett.* 19[24] (2000) 2209-2211.
16. L. Le Guéhennec, A. Soueidan, P. Layrolle, and Y. Amouriq, *Dent. Mater.* 23[7] (2007) 844-854.
17. M. Guazzato, M. Albakry, L. Quach, and M.V. Swain, *Biomaterials.* 25[11] (2004) 2153-2160.
18. K. Pardun, L. Treccani, E. Volkmann, P. Streckbein, C. Heiss, G.L. Destri, G. Marletta, and K. Rezwani, *Mater. Sci. Eng. C.* 48 (2015) 337-346.
19. O.E. Ogle, *Dent. Clin. North Am.* 59[2] (2015) 505-520.
20. H.J. Kim, J.J. Kim, and J.K. Lee, *J. Nanosci. Nanotechnol.* 19[10] (2019) 6285-6290.
21. D. Hanft, J. Exner, M. Schubert, T. Stöcker, P. Fuierer, and R. Moos, *J. Ceram. Sci. Technol.* 6[3] (2015) 147-182.
22. J. Akedo, *Mater. Sci. Forum.* 449-452 (2004) 43-48.
23. Y. Imanaka, and J. Akedo, in *Proceedings of the 54th Electronic Components and Technology Conference*, April 2004, edited by IEEE (Institute of Electrical and Electronics Engineers, 2004) p. 1614.
24. J. Akedo, *J. Therm. Spray. Technol.* 17[2] (2008) 181-198.
25. D.W. Lee, and S.M. Nam, *J. Ceram. Process. Res.* 11[1] (2010) 100-106.